Greedy Principal Flows

National University of Singapore

Sebastian Lie

05 March 2021

Acknowledgements

My 7 soft toys. And my desk lamp for being the light of my life.

Abstract

Principal Flows are a great tool to use when we want to extend the notion of Principal Component Analysis to multivariate high dimensional data that lie on non-linear lower dimensional manifolds. This is especially since principal flows are curves on a manifold that move along a path of maximal variation of the data, and capture forms of variation that would escape Principal Component Analysis. Principal flows were originally obtained by solving a problem in variational calculus using the Euler-Lagrange method. In this thesis, we explore the use of a novel, simpler approach to constructing principal flows: a greedy approach. Furthermore, since after rotation, centering, translation and normalisation, vectors can be viewed as points on the hypersphere, we restrict this problem to constructing principal flows on hypersphere. Let us call this new approach the greedy principal flow. We test the effectiveness of our new principal flow on toy data, and explore the patterns of variation it finds in real world data. Our results show that our greedy principal flow retains the same effectiveness as the original, and finds new, meaningful patterns in existing real world data.

Contents

List of Figures

Chapter 1

Introduction

1.1 Motivation

With the advent of Big Data, and the rise in popularity of data science, machine learning has been used successfully to solve a variety of problems, such as regression and classification problems. However, machine learning can also be used in a more subtle, but no less important way: to discover patterns in the data and glean more information from it. Among methods that have this aim, Principal Component Analysis is the most popular, taught in almost every machine learning course. It does however, have a glaring weakness: it does not perform well when the data we are working with is sampled from a non-linear manifold.

This, however is remedied with the principal flow algorithm: it constructs a curve that at each local point moves in the direction of maximal variation and retains canonical PCA interpretation in euclidean space. Yet, this method is not easy to obtain, having to solve a problem in variational calculus. What if we could construct this curve with a greedy approach? Could the curve constructed still function as a principal flow? How would it perform on real world data and what new patterns of variation could it yield? These are some of the questions that motivated this thesis.

The first chapter outlines notations and some technical definitions. The second is a literature

review of popular methods in dimension reduction. The third is where we explain how the greedy principal flow is constructed and the fourth chapter is where we present and analyse our results after applying the greedy principal flow on toy and real world data.

1.2 Notation

Notation	Explanation
$\mathbb{R}^D$	D dimensional euclidean space.
$\mathbf{X}$	Data matrix of dimensions $n \times D$
$\mathbf{X}_c$	Centered Data matrix of dimensions $n \times D$
D	Dimension of the high-dimensional data.
d	Dimension of the manifold embedded in D dimensional space
$\mathcal{M}^d$	A connected and complete d-dimensional manifold embedded in $\mathbb{R}^D$
p	A point on the manifold, $\mathcal{M}^d$.
$\mathbf{v}$	A vector.
$T_p\mathcal{M}$	The Tangent space of a point p on $\mathcal{M}^d$.
$\mathbf{C}$	A Covariance matrix.
$\mathbf{C}_h(p)$	A local tangent covariance matrix with scale h of data on $T_p\mathcal{M}$.
$\{x_1, ...x_n\}$	A collection of n data points in D dimensions. They are also the rows of $\mathbf{X}$
$\mathbf{1}$	A vector of 1s.
$\mathbf{I}$	The identity matrix.
$\mathbf{X}^T$	Transpose of $\mathbf{X}$.
$\mathbf{X}_{(d)}$	d dimensional representation of $\mathbf{X}$
$\mathbf{V}$	The matrix of eigenvectors of $\mathbf{C}$, where eigenvectors are columns and are sorted in descending order of their eigenvalues.
$\mathbf{\Lambda}$	The diagonal matrix of eigenvalues of $\mathbf{C}$, sorted in descending order.
$\mathbf{V}_{(d)}$	d dimensional representation of $\mathbf{X}$
$\mathbf{S}$	Squared dissimilarity matrix of the data in $\mathbf{X}$ of dimension $n \times n$, calculated with euclidean distance.
$\otimes$	Outer Product

1.3 Definitions

1.3.1 Vector Fields

A vector at point $\mathbf{x}$, $\mathbf{x} \in \mathbb{R}^D$ is a pair $\mathbf{a} = (\mathbf{x}, \mathbf{v})$, $\mathbf{v} \in \mathbb{R}^D$, such that $\mathbf{v}$ is the vector $\mathbf{v}$ translated so that its tail is at $\mathbf{x}$ instead of the origin. All vector operations are defined such that the first item of the pair remains the same, and the second item is the result of the operation. The length and angle between two vectors are the same as normal vectors rooted in the origin.

Definition: A *vector field* $\mathbf{F}$ on $U \subset \mathbb{R}^D$ is a function which assigns to each point of U a vector at that point. Then

$$\mathbf{F}(\mathbf{x}) = (\mathbf{x}, F(\mathbf{x}))$$

for some function $F : U \longrightarrow \mathbb{R}^D$. Vector fields on $\mathbb{R}^D$ are often most easily described by specifying this associated function F. A pictoral example of a vector field is below.

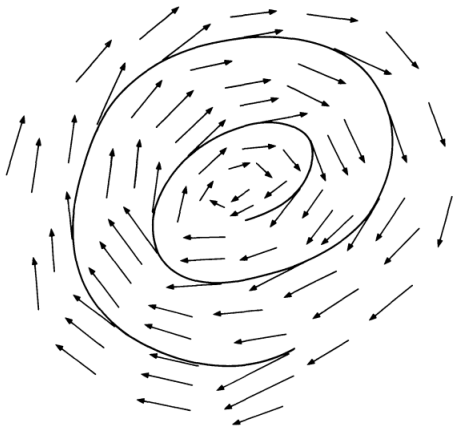

Figure 1.1: An example of a vector field, $\mathbb{R}^3$

1.3.2 Logarithm Maps

Logarithm Map: For each $p \in \mathcal{M}^d$, let

$$log_p(x) : \mathcal{M}^d \longrightarrow T_p\mathcal{M}$$

be the logarithm map. The log map is a function that projects a point x on the manifold $\mathcal{M}^d$ onto $T_p\mathcal{M}$, by producing a vector on $T_p\mathcal{M}$ which indicates the direction in which p should move to obtain the projection of $x \in \mathcal{M}^d$ onto $T_p\mathcal{M}$.

Exponential Map: For each $p \in \mathcal{M}^d$, let

$$exp_p(\mathbf{v}) : T_p\mathcal{M} \longrightarrow \mathcal{M}^d$$

be the exponential map. Exponential maps are the inverse of the logarithm maps. Let the vector $\mathbf{v}$ be the vector from p to the point t on $T_p\mathcal{M}$ we wish to project onto $\mathcal{M}^d$. Then the exponential map moves along the geodesic on $\mathcal{M}^d$ that mirrors the direction of $\mathbf{v}$ on $T_p\mathcal{M}$ and finds the projection of t on $\mathcal{M}^d$.

1.3.3 Tangent Space

To define the tangent space we refer to the diagrams below.

Let the sphere be the manifold, $\mathcal{M}^d$, and let $T_p\mathcal{M}$ be the plane tangent to $\mathcal{M}^d$. Let the blue point be p. This is to say that the tangent space of some manifold $\mathcal{M}^d$ log_p would then project points from $\mathcal{M}^d$ to the hyperplane, and exp_p would project points from $T_p\mathcal{M}$, the hyperplane, to $\mathcal{M}^d$. Any vectors lying in this hyperplane are in the tangent space, of $\mathcal{M}^d$ at p.

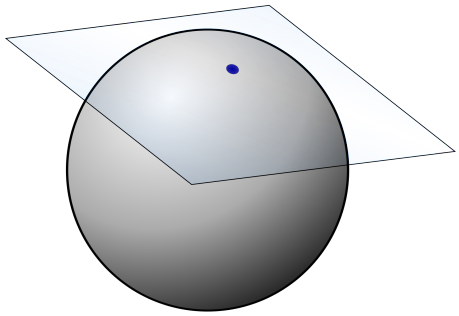

(a) Tangent Space of a Sphere
Obtained from [8]

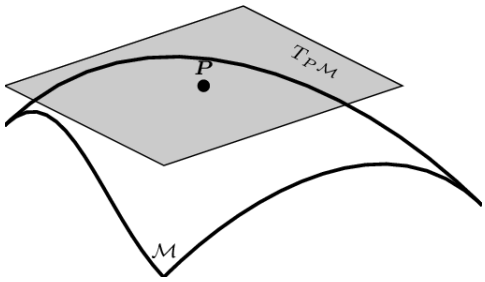

(b) Close-up of the Tangent space in (a),
Obtained from [7]

Figure 1.2: Illustration of a Tangent Space

1.3.4 Geodesics

Geodesics are curves on $\mathcal{M}^d$ which play the same role as straight lines in $\mathbb{R}^d$. They can be thought of as the "shortest path" between two points on the manifold, $\mathcal{M}^d$.

The Euclidean distance between two points p, q is defined as $\|p - q\|$, or the 2-norm of the vector $p - q$. Geodesic distance extends this concept of Euclidean, straight line distance in the Euclidean space to Manifolds.

1.3.5 Eigenvalues and Eigenvectors

Definition: Let $\mathbf{C} \in \mathbb{R}^{D \times D}$. Then a non-zero vector $\mathbf{v}$ is an eigenvector of $\mathbf{C}$ if there exists some scalar λ such that $\mathbf{Cv} = \lambda\mathbf{v}$. Then λ is known as the eigenvalue corresponding to vector $\mathbf{v}$.

Here we also note that for any two eigenvectors v_i and v_j, $i \neq j$, $v_i \cdot v_j = 0$, or any two eigenvectors are orthogonal to each other, and that $v_i \cdot v_i = 1$.

1.3.6 Diagonalisation

We say that a matrix, $\mathbf{C}$, is diagonalisable if there exists an orthonormal matrix such that the rows of that orthonormal matrix are the eigenvectors of $\mathbf{C}$, and a diagonal matrix $\mathbf{\Lambda}$ whose diagonal entries are the eigenvalues of $\mathbf{C}$. In the context of this report, we only consider the

eigendiagonalisation of some covariance matrix $\mathbf{C} \in \mathbb{R}^{D \times D}$, which is symmetric and thus, always diagonalisable. Formally, the eigendiagonalisation of $\mathbf{C}$ is given by:

$$\mathbf{C} = \mathbf{V}\mathbf{\Lambda}\mathbf{V}^T$$

Chapter 2

Literature Review

2.1 Linear Dimension Reduction

2.1.1 Principal Component Analysis

Principal Component Analysis(PCA) tries to obtain a lower-dimensional representation of the data that retains as much variation as possible present in the data set. PCA relies on constructing principal components (PCs): new variables that are linear combinations of the original variables that have first been centered. These PCs are uncorrelated (orthogonal) and ordered in descending order by the amount of variability of the original data retained. Thus, PCA reduces some high-dimensional data of dimension D to d by computing the first d PCs.

We compute these PCs by first centering the data matrix, $\mathbf{X}$, and obtaining $\mathbf{X}_c$. Next we compute the covariance matrix of the centered data matrix: $\mathbf{C}$. Then we compute the eigendiagonalisation of $\mathbf{C}$, and obtain $\mathbf{V}_d$, the d eigenvectors associated with the d largest eigenvalues. Here, we note that these d eigenvectors are the d principal directions: directions onto which data is projected to obtain the d PCs. Finally, we construct the d PCs by computing $\mathbf{X}\mathbf{V}_d$.

The PCA algorithm is outlined below. We assume for simplicity that the following functions

are available: *center* that centers a given matrix, *covariance* that computes the covariance of a given matrix, and *diagonalise* which compute the d eigenvectors associated with the d largest eigenvalues.

Algorithm 1: PCA($\mathbf{X}$, d)

Result: $\mathbf{X}_{(d)}$, the d dimensional representation of $\mathbf{X}$, which are the d PCs
$\mathbf{X}_c = center(\mathbf{X})$;
$\mathbf{C} = covariance(\mathbf{X}_c)$;
$\mathbf{V}_d = diagonalise(\mathbf{C}, d)$;
$\mathbf{X}_{(d)} = \mathbf{X}\mathbf{V}_d$;
return $\mathbf{X}_{(d)}$

2.1.2 Classical MDS, Euclidean Distance

Multidimensional Scaling (MDS)'s main aim is find some d dimensional representation of the original data, $\mathbf{X}_{(d)}$, that minimises the discrepancy between the pairwise distances of $\mathbf{X}$ and $\mathbf{X}_{(d)}$, given the squared matrix of pairwise distances of $\mathbf{X}$, $\mathbf{S}$.

Since dissimilarities do not change under translations, we can assume that $\mathbf{X}$ has column means equal to 0. Let $\mathbf{B} = \mathbf{X}\mathbf{X}^T$ be the gram matrix. Let $\mathbf{J}$ be the centering matrix: $\mathbf{J} = \mathbf{I} - n^{-1}\mathbf{1}\mathbf{1}^T$, where $\mathbf{I} \in \mathbb{R}^{n\times n}$ and $\mathbf{1} \in \mathbb{R}^{n\times 1}$ Then, we run MDS by first computing $\mathbf{B} = -\frac{1}{2}\mathbf{J}\mathbf{S}\mathbf{J}$. Then computing the eigendecomposition of $\mathbf{B}$. $\mathbf{B} = \mathbf{V}\mathbf{\Lambda}\mathbf{V}^T$. From the original $\mathbf{V}$ we take the first d columns: $\mathbf{V}_d$ and the first $d \times d$ submatrix of $\mathbf{\Lambda}$: $\mathbf{\Lambda}_d^{1/2}$. Finally, we compute $\mathbf{X}_{(d)} = \mathbf{V}_d\mathbf{\Lambda}_d^{1/2}$ to obtain the d-dimensional representation of the original data, $\mathbf{X}$. The MDS algorithm is outlined below. Assume we have a function *diagonalise* which computes returns the first d columns of $\mathbf{V}$ and the $d \times d$ submatrix of $\mathbf{\Lambda}$.

Note that using Euclidean distances, the result of MDS is the same as PCA.

Algorithm 2: MDS($\mathbf{S}$, d)

Result: $\mathbf{X}_{(d)}$, the d dimensional representation of $\mathbf{X}$
$\mathbf{J} = \mathbf{I} - n^{-1}\mathbf{1}\mathbf{1}^T$;
$\mathbf{B} = -\frac{1}{2}\mathbf{J}\mathbf{S}\mathbf{J}$;
$\mathbf{V}_d, \mathbf{\Lambda}_d = diagonalise(\mathbf{B}, d)$;
$\mathbf{X}_{(d)} = \mathbf{V}_d \mathbf{\Lambda}_d^{1/2}$;
return $\mathbf{X}_{(d)}$

2.2 Non-Linear Dimension Reduction

Non-linear dimensionality reduction methods are particularly useful when the multivariate data we obtain is sampled from a smooth non-linear manifold $\mathcal{M}^d$, e.g a manifold in an S-shape or a hypersphere. This class of methods obtain better estimates than linear methods like PCA and MDS, especially for the data mentioned above. They are especially successful as certain data sets contain essential nonlinear structures that are invisible to PCA and MDS.

2.2.1 Isomap

Isomap, introduced by Tenenbaum et al. [3] is an extension of MDS to manifolds in which embeddings are optimized to preserve geodesic distances between pairs of data points. It combines the major algorithmic features of PCA and MDS — computational efficiency, global optimality, and asymptotic convergence guarantees — with the flexibility to learn a broad class of nonlinear manifolds. Isomap achieves this by estimating the geodesic distance between data points, given only input-space distances, e.g euclidean distance between points. This relies on the fact that for neighboring points, input-space distance provides a good approximation to geodesic distance. For faraway points, Isomap approximates geodesic distance by adding up a sequence of "short hops" between neighboring points, computed efficiently by finding shortest paths in a graph with edges connecting neighboring data points. Like MDS, Isomap takes as input $\mathbf{S}$ but differs by first constructing the neighbourhood graph, G. We start by creating nodes for every data point i. Given some user input K, for every point i, Isomap adds an edge between the i and another point j with weight $S_{i,j}$ if j is one of i's K nearest neighbours. We then run an all pairs shortest path algorithm on G (we use FloydWarshall here), and obtain a new matrix $\mathbf{A}$, where $\mathbf{A}_{i,j}$ is the shortest distance from i to j. This approximates geodesic distance between i and j. Then we run $MDS(\mathbf{A}, d)$ from to obtain $\mathbf{X}_{(d)}$.

The algorithm is outlined below. For simplicity, assume we have a function *ConstructGraph* which constructs the graph G as explained above.

Algorithm 3: Isomap($\mathbf{S}$, d, K)

Result: $\mathbf{X}_{(d)}$, the d dimensional representation of $\mathbf{X}$
$G = ConstructGraph(\mathbf{S}, K)$;
$\mathbf{A} = FloydWarshall(G)$;
return *MDS(*$\mathbf{A}$*, d)*

2.2.2 Locally Linear Embeddding

Locally Linear Embedding (LLE) introduced by Saul and Roweis [6] aims to construct a mapping from the D dimensional original points to the d dimensional reconstructed points that preserves the local configurations of each point's nearest neighbors. Locally, LLE assumes the embedding is linear, and for each data point $p \in \mathbb{R}^D$, LLE uses a linear combination of its K nearest neighbours to reconstruct a lower-dimensional $p_d \in \mathbb{R}^d$.

Let the set of the i-th point's k nearest neighbours be N_k^i. LLE starts by learning some weights from the D-dimensional data: $\mathbf{W}$ by minimizing the **Reconstruction Error** below using constrained linear fits.

$$\varepsilon(\mathbf{W}) = \sum_{i}^{n} |\mathbf{X}_i - \sum_{j \in N_k^i}^{K} \mathbf{W}_{ij}\mathbf{X}_j|^2$$

Here, $\mathbf{W}$ are the weights that best reconstruct each data point from it's K neighbours, and $\mathbf{W}_{ij}$ represents the contribution of the j-th data point in reconstructing the i-th one. These weights obey an important symmetry: for any particular data point, they are invariant to rotations, rescalings, and translations of that data point and its neighbors. They thus reflect intrinsic geometric properties of the data that are invariant to such transformations, and therefore, we expect their characterization of local geometry in the original data space to be equally valid for local patches on the manifold. This is what motivates our use of $\mathbf{W}_{ij}$ in reconstructing the embedded manifold coordinates in d dimensions.

Next, compute the vectors $\mathbf{Y}_i$ best reconstructed by the weights $\mathbf{W}_{ij}$ by choosing the d dimensional coordinates of each output that minimise the **Embedding Cost Function**:

$$\Phi(\mathbf{Y}) = \sum_{i} |\mathbf{Y}_i - \sum_{j} \mathbf{W}_{ij}\mathbf{Y}_j|^2$$

At the end of LLE, each D-dimensional observation $\mathbf{X}_i$ is mapped to a d dimensional $\mathbf{Y}_i$ representing global internal coordinates on the manifold.

Algorithm 4: LLE($\mathbf{X}$, d, k)

Result: $\mathbf{X}_{(d)}$, the d dimensional representation of $\mathbf{X}$
First compute N_k^i for all x_i;
$\mathbf{W} = argmin_{\mathbf{W}} \sum_i^n |x_i - \sum_{j \in N_k^i}^k \mathbf{W}_{ij} x_j|^2$;
$\mathbf{X}_{(d)} = argmin_{\mathbf{Y}} \sum_i |\mathbf{Y}_i - \sum_{j \in N_k^i}^k \mathbf{W}_{ij} \mathbf{Y}_j|^2$;
return $\mathbf{X}_{(d)}$

2.2.3 Principal Geodesic Analysis

Principal Geodesic Analysis(PGA) introduced here [2], is a generalization of PCA to manifolds. The main aim of PGA is to describe some D dimensional data that lie on $\mathcal{M}^d$ embedded in $\mathbb{R}^D$. Let $T_p\mathcal{M}$ be the tangent space of $\mathcal{M}^d$ at the intrinsic mean p of the data. The intrinsic mean here is the extension of the concept of the mean in euclidean space to manifolds. PGA aims to construct some principal geodesics that are analogous to principal directions in PCA: the directions along which data is projected to obtain a PC.

Instead of finding the principal geodesic however, Fletcher et al. prove that we can approximate the d geodesics along which maximal variation lies by projecting data from $\mathcal{M}^d$ to $T_p\mathcal{M}$ where p is the intrinsic mean of $\{x_1, ..x_n\}$ and then finding the d eigenvectors associated with the d largest eigenvalues of the covariance matrix of the projected data.

PGA begins with computing p by first setting p to a random data point, then iteratively obtaining a better estimate of p. Let p_i be the estimate of p at the i-th iteration. At the i-th iteration, we compute the average of the vectors obtained using the $log_{p_{i-1}}(x_i), \forall x_i$ then setting p_i as the projection of that average using $exp_{p_{i-1}}$.

After obtaining p, we calculate the vectors $u_i = log_p(x_i),\ \forall x_i$. Next we calculate the covariance matrix $\mathbf{C} = \frac{1}{n} \sum_{i=1}^n u_i u_i^T$. Finally we diagonalise $\mathbf{C}$ to obtain $\{v_k, \lambda_k\}$ the eigenvectors and eigenvalues respectively, which represent the principal directions in the tangent space $T_p\mathcal{M}$ and the variances. The algorithm for PGA is outlined below.

Algorithm 5: PGA($\{x_1, ...x_n\}$)

Result: $\{v_1, ...v_D\} \in T_p\mathcal{M}$, principal directions and
Variances $\{\lambda_1, ...\lambda_D\} \in \mathbb{R}$
$p =$ intrinsic mean of data $\{x_1, ...x_n\}$;
$u_i = log_p(x_i)$;
$\mathbf{C} = \frac{1}{N}\sum_{i=1}^{N} u_i u_i^T$;
$\{v_1, ...v_D\}, \{\lambda_1, ...\lambda_D\} =$ eigenvectors and eigenvalues of $\mathbf{C}$;
return $\{v_1, ...v_D\}, \{\lambda_1, ...\lambda_D\}$

Chapter 3

Greedy Principal Flows

3.1 Goal Of Research

The main objective for greedy principal flows is to quantify or describe multivariate data on the manifold: we cannot simply fit a line, as this is not Euclidean space. Instead, we want some curve or path such that, locally, it follows the path of maximal variation of the data in some neighbourhood, but globally also provides the path of maximal "cumulative" variation of the data. This problem has already been solved in [5], where the principal flows were constructed by solving a problem in variational calculus. Here we note that we focus on the first order principal flow, which can be thought of as the manifold extension of the first PC in euclidean space. Therefore, we focus instead on constructing the principal flow using a novel, simpler to implement approach: a greedy algorithm. Additionally, we simplify our approach further and assume that our data $\mathbf{X}$ is some D dimensional data lying on a hypersphere $\mathcal{M}^d$. Thus, formally, our goal is to implement this simpler version of the principal flow algorithm in a popular programming language, and experiment with the results that this implementation of the principal flow algorithm. How would it describe various, popular multivariate datasets? Could it find novel ways of describing popular, existing high-dimensional data?

3.2 Centroid Algorithm

Before we get into our principal flow algorithm, we first need to establish our starting point. Since our principal flow follows the path of maximal variation of our data, we know it should pass through the centroid of the data. Thus, we first aim to estimate this centroid and use it as a starting point. Although there are many ways of doing this, including the method to find the intrinsic mean in chapter 2.2.3, we opt to make use of the fact that the first PC passes through the centroid of the data. Thus, if we iteratively project all the data onto the tangent space of the hypersphere, find the 1st principal direction, move in that direction, and find the projected point on the hypersphere, we will eventually converge on the centroid. The algorithm to find the centroid is outlined below.

Algorithm 6: Centroid($\{x_1, ...x_n\}$)

Result: p, centroid of the data
$p =$ a random data point from $\{x_1, ...x_n\}$;
for $i = 1 \rightarrow max\_iter$ **do**
  Compute $u_i = log_p(x_i)$ for all x_i,;
  $\mathbf{C} = \frac{1}{N}\sum_{i=1}^{N} u_i u_i^T$;
  $v_1 =$ eigenvector corresponding to the largest eigenvalue of $\mathbf{C}$;
  $p' = p + \epsilon v_1$;
  $p = exp_p(p')$;
return p

3.3 Algorithm

Now we move on to outlining and elaborating on the Principal flow algorithm. Starting from the centroid of the data set, we first project $\mathbf{X}$ onto the hyperplane at p (initially the centroid of the data lying on $\mathcal{M}^d$), $T_p\mathcal{M}$. Here we may choose to project all our data, or use a kernel function, $\mathcal{K}$ to weight our data so that more emphasis is placed on points in some neighborhood around p, whose size is controlled by scale parameter h, than outside it. Intuitively, h controls how sensitive the principal flow is to local data. For our algorithm,

we implement three choices of kernel functions: The binary kernel which weights points as one or zero depending on their distance from p, the gaussian kernel which weights points according to the gaussian distribution based on their distance from p and lastly the identity kernel, which sets all weights to be one.

Thus, we first apply our kernel function to the data, and obtain weights $\{w_i, ...w_n\}$, then apply our log map log_p to project our data on $\mathcal{M}^d$ obtaining a matrix of vectors on the tangent plane that point from p to the projected points. These are our plane vectors $log_p(x_i)$.

Then we compute the covariance matrix of the plane vectors using both our weights and our plane vectors by the equation below obtained from [5].

$$C_h(p) = \frac{1}{\Sigma_i \mathcal{K}_h(x_i, p)} \sum_{i=1}^{n} (log_p(x_i) \otimes log_p(x_i)) \mathcal{K}_h(x_i, p)$$

We then perform eigendiagonalisation of the covariance matrix. Take the eigenvector v_1 corresponding to the largest eigenvalue λ_1. This indicates the direction of the principle flow. Let us call it the principal direction. Here, λ_1 corresponds to the amount of variance of our data in the direction of v_1. This is where the "greediness" in our algorithm lies: since we choose at each step, the direction of maximum variance.

If this is the first iteration, we collect two points: one point when we move a step size of ϵ in the principal direction, and the other when we move a step size of ϵ in the opposite of the principal direction. We then project both points back onto $\mathcal{M}^d$, using exp_p. Set p to be the first point, and p_opp to be the second. Otherwise, we check that this principal direction is in the same direction as the previous principal direction, and if not, apply a negative sign to the principal direction. As above we now move a step size of ϵ in the principal direction, then project both points back onto $\mathcal{M}^d$, using exp_p.

We repeat the procedure above until the maximum iterations is reached. Then we set $p = p\_opp$ and repeat the procedure above, with the exception that we only produce one point at every iteration. This is to say, we only repeat what is done in the second iteration

onwards, and stop when the maximum number of iterations is reached. The Greedy Principal Flow algorithm is outlined below.

Algorithm 7: GreedyPrincipalFlow($\{x_1, ...x_n\}$, $\mathcal{K}$, max_iter, h, ϵ)

Result: p_i, points on the principal flow
for $i = 1 \rightarrow max\_iter$ **do**
  if $i == 1$ **then**
    $\{w_i, ...w_n\} = \mathcal{K}(h, p, \{w_i, ...w_n\}$;
    $\mathbf{C}_h(p) = \frac{1}{\Sigma_i w_i} \sum_{i=1}^{n} (log_p(x_i) \otimes log_p(x_i))w_i$;
    $\{v_1, ..., v_n\}, \{\lambda_1, ...\lambda_n\} = diagonalise(\mathbf{C}_h(p))$;
    $first\_direction = v_1$;
    $p = exp_p(p + \epsilon v_1)$;
    $p\_opp = exp_p(p - \epsilon v_1)$;
    $v_1\_past = v_1$;
  else
    $\{w_i, ...w_n\} = \mathcal{K}(h, p, \{w_i, ...w_n\}$;
    $mathbfC_h(p) = \frac{1}{\Sigma_i w_i} \sum_{i=1}^{n} (log_p(x_i) \otimes log_p(x_i))w_i$;
    $\{v_1, ..., v_n\}, \{\lambda_1, ...\lambda_n\} = diagonalise(\mathbf{C}_h(p))$;
    if $cos^{-1}(v_1^T v_1\_past > \pi/2$ **then**
      $v_1 = -v_1$;
    $p = exp_p(p + \epsilon v_1)$ update p;
$p = p\_opp$;
for $i = 1 \rightarrow max\_iter$ **do**
  $\{w_i, ...w_n\} = \mathcal{K}(h, p, \{w_i, ...w_n\}$;
  $mathbfC_h(p) = \frac{1}{\Sigma_i w_i} \sum_{i=1}^{n} (log_p(x_i) \otimes log_p(x_i))w_i$;
  $\{v_1, ..., v_n\}, \{\lambda_1, ...\lambda_n\} = diagonalise(\mathbf{C}_h(p))$;
  if $cos^{-1}(v_1^T v_1\_past > \pi/2$ **then**
    $v_1 = -v_1$;
  $p = exp_p(p + \epsilon v_1)$;
return p

3.4 Extension: Greedy Principal Boundary

In the section above, we have already seen the principal flow. Now we extend the idea of Principal flows to attempt to find some boundary of the data. Let us assume that the data is contained on some ellipse of the manifold $\mathcal{M}^d$. Then our aim is to find some boundary around this ellipse. We proceed similarly to the principal flow, except that we now save $v_1, v_2, \lambda_1, \lambda_2$ when we diagonalise $\mathbf{C}_h(p)$. and use them to compute the boundaries of data. Then at each iteration, the boundary b is calculated before p is updated by $b_1 = exp_p(p + \frac{\lambda_2}{\lambda_1} * radius * v_2)$ and $b_2 = exp_p(p - \frac{\lambda_2}{\lambda_1} * radius * v_2)$ where radius is a user specified parameter. Intuitively, we try to move a distance in the direction of v_2 orthogonal to the principal flow that approximates the radius of the ellipse that contains the data, $\mathbf{X}$.

Chapter 4

Applications

Writing the algorithm is meaningless without testing that it also functions as we want it to. First we start with simple applications on toy data to confirm that our algorithm works as intended, then we apply it on some real world data to show how the principal flow can be used there as well.

4.1 Toy Data

4.1.1 Without Noise

As a sanity check or proof of concept of our principal flow, we first want to test our algorithm on some toy data that we know lies on the three-dimensional unit sphere. This will help us visualise the flow created and determine if it follows the pattern of the data, and thus act as a proof of concept of our algorithm. We generate some data artificially.

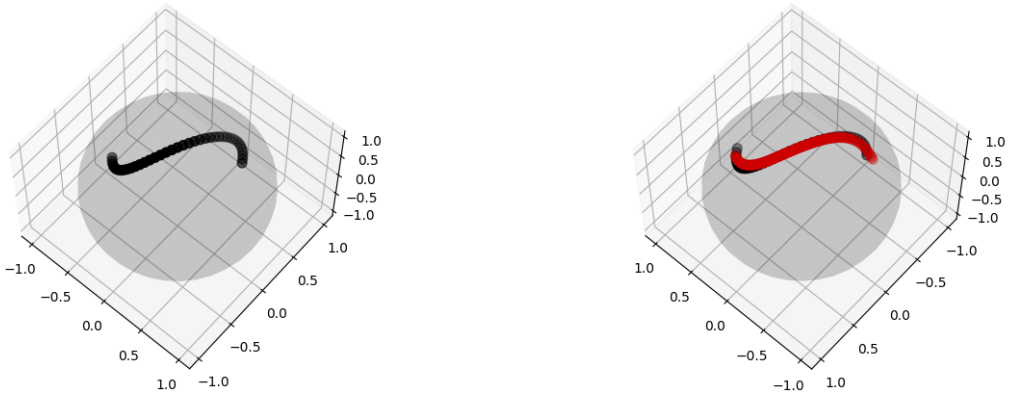

(a) Toy data 13, $\mathbb{R}^3$ (b) Principal Flow on Toy Data, $\mathbb{R}^3$

Figure 4.1: Principal flow, no noise

For example, this dataset is created by setting the first coordinate of the i-th point, $x_{i,1} = \frac{i-n/2}{n}$, then $x_{i,2} = sin(4 * x_{i,1})/2$, and the third to $x_{i,3} = \sqrt{1 - x_{i,1}^2 - x_{i,2}^2}$, where n is the number of points we want to generate.

Now that we have seen the Toy Data, let us apply the Principal Flow algorithm to the data above. This 3D plot shows the original data in black, and the principal flow in red. With some tuning of h, the size of the neighbourhood, we can see that we have constructed a principal flow that follows the original data almost exactly, reconstructing an S with some slight differences at the curves of the s-shape of the original data. We have now seen that proof that our principal flow algorithm works: it is able to accurately reconstruct the toy data, the s curve on the sphere.

4.1.2 With Noise

Next, gaussian noise was added to the S-shaped data on the sphere to create a noisy dataset. Then we fitted a principal flow to this noisy data.

We can see that the principal flow obtained seems to follow the new pattern of variation in the data: from the more dense cloud of points on the left, to the curve of the points in the center to the other dense cloud of points on the right. We can see from these examples

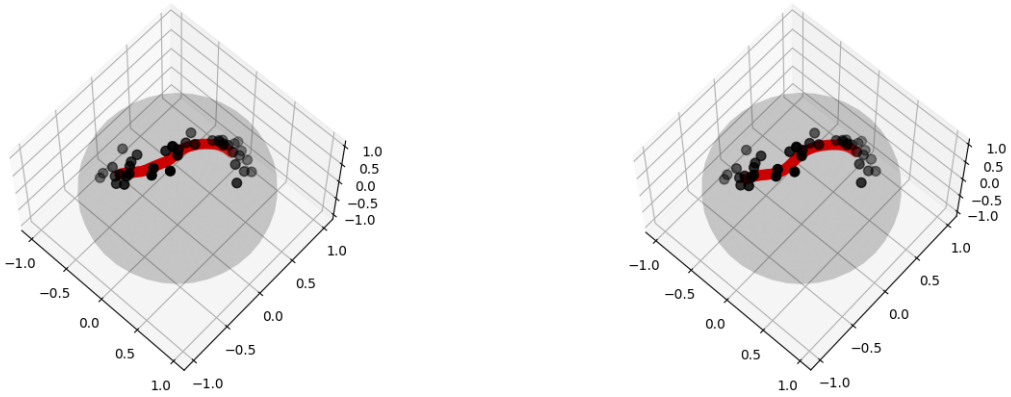

(a) Flow on Noisy Data using binary kernel (b) Flow on Noisy Data using gaussian kernel

Figure 4.2: Principal flow, noisy data

that even with noise, our algorithm is able to discern the pattern of the data.

4.1.3 Boundary Flow with Noise

Next we test out our extension, our algorithm for our principal boundary. Since we need a "cloud" of data, we apply some gaussian noise on the data from above, and then run our principal boundary algorithm on it. Let the principal flow be the curve in red, and the boundaries be in blue and green.

With some tuning, we obtain these three curves: we can see that the principal flow is in the middle of the dataset, while the boundary flows accompany it in parallel and even form to the shape of the cloud of data, bending outwards when there is a point beyond it. Through this graph, we can see how the principal boundary can work and be shaped by the shape of the cloud of data.

4.2 Real World Data

Our results on artificial data are promising, however, it means little if there are no real-world applications for our greedy principal flow.

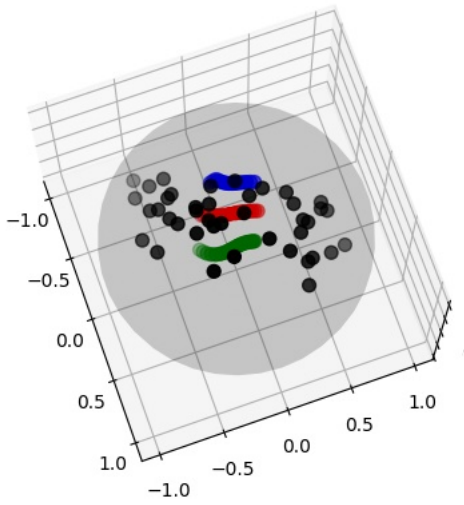

Figure 4.3: Boundary Flow on noisy data

4.2.1 MNIST

We first test the principal flow algorithm on the MNIST dataset, a rite of passage for machine learning algorithms. The MNIST dataset is a set of handwritten digits.

These images, read from left to right, top to bottom, are points from the greedy principal flow using the binary kernel. Although it does not represent all the variability of the 3s in the dataset, we can see that all the images obtained are "nice" representations of 3s, in that they cannot be confused with any other digit, and they seem to be relatively neatly written. Within these "nice" 3s then we observe the source of the variability: the "slant" of the digit. We can see that the digits start out leaning right with the upper left group of images, and slowly rotates to slant to the left, going through a phase of being perfectly centered, while the tails of the images seem not to move at all.

This perhaps is an insight into the well-written 3s in the dataset and perhaps of neat handwritten digits in general: that the upper and middle part of the digit differ mainly in ori-

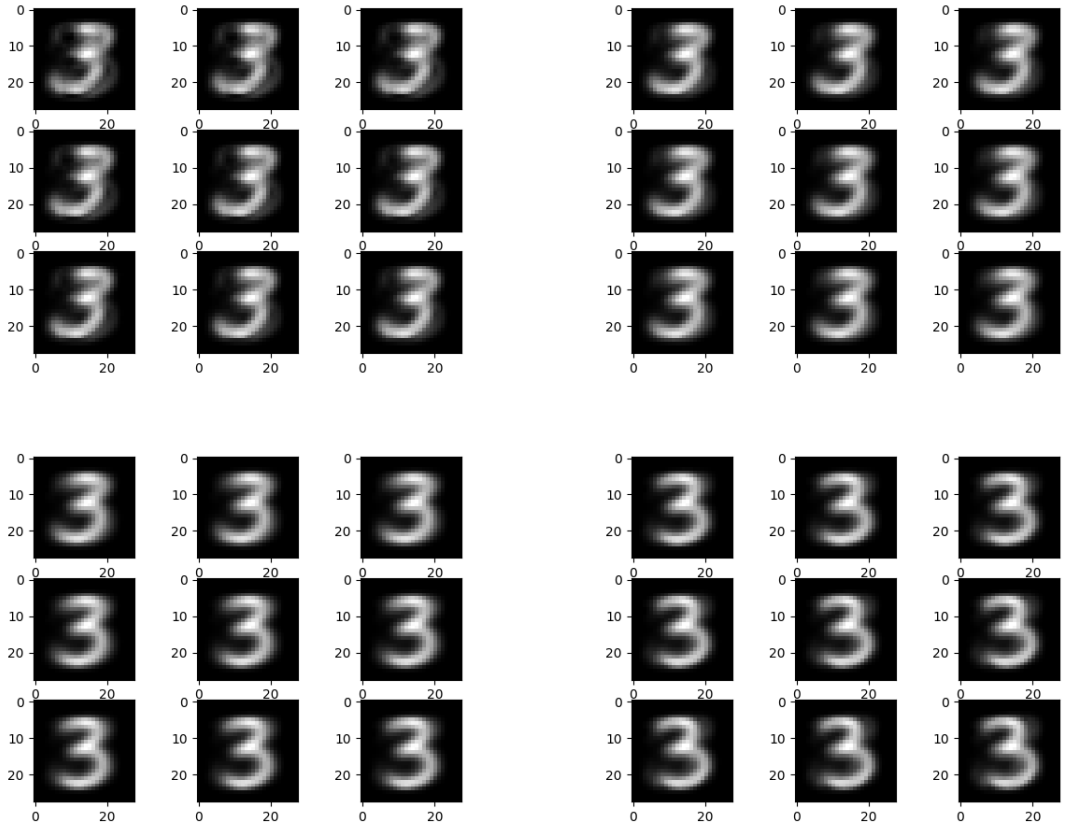

Figure 4.4: MNIST Flows, from left to right.

entation, while the tail remains mostly fixed. Additionally, the fact that the 3s from the principal flow are neat representations of the digit, and the gradual change in orientation of the digit along the curve suggests that our greedy principal flow has found a path that has some intuitive meaning. This supports our use of the greedy principal flow to understand our data better, and seek out some pattern of variation that we might otherwise be oblivious too. It also perhaps justifies our choice of a hypersphere for $\mathcal{M}^d$.

4.2.2 Olivetti faces

Next we test our algorithm on a facial dataset. The Olivetti face dataset is old, and thus images are small, and only in black and white. This however is an advantage, as smaller images help the principal flow algorithm run faster, allowing us to experiment with a variety of parameters.

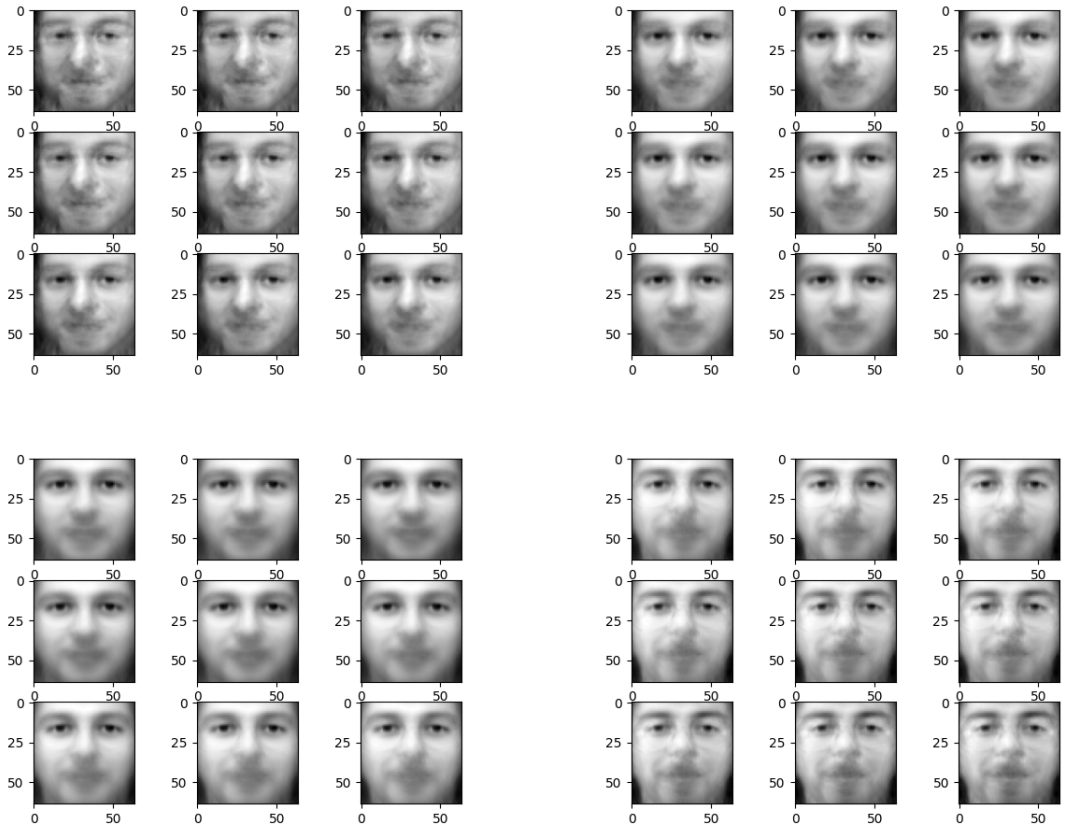

Figure 4.5: Flow for Olivetti face data, from left to right.

Although disturbing, we can see the results of our algorithm. We obtain mostly clear pictures of faces, with faces differing in whether they wear glasses (first few images on upper left) or the angle of their face, or whether they have a beard (last two images, bottom right). Indeed we observe that the difference between the men and woman in the data are not as

stark as the difference between bearded and non-bearded individuals. This again indicates the strength of our algorithm: it is able to suss out the main way in which these images vary. Additionally, we can glean meaning from neighbouring images on the curve: they are close to each other in a meaningful way. This can be seen from how the set of faces on the upper left are slightly tilted away from us, but gradually transition to facing us in the bottom left set of images. The fact that the images on the principal flow transition smoothly tell us that on the principal flow, a face slightly tilted away is near a face directly facing the camera which makes intuitive, real world sense. This is an indication that our choice of $\mathcal{M}^d$ does yield fruit and have some real world meaning, and that our principal flow seems to preserve some real world interpretation and meaning as it transitions smoothly through the orientation of faces in the data.

Future Directions

The topic of principal flows and manifold learning in general is a rich field with much potential, and there are many avenues of expanding the work done in this report. One potential direction is constructing the k-th order principal flows, where $k > 1$. Another potential avenue of research is using different kinds of $\mathcal{M}^d$. In this report, we have restricted ourselves only to the hypersphere. Although this might be a "good enough" approximation, if we had intuition about the specific form of the manifold on which our multivariate data lies, and we determine that the hypersphere is unsuitable, then this current principal flow would not be able to accomodate this intuition. With a different manifold, we might be able to obtain a different principal flow that might give us more information about the variability of the data and describe it more appropriately than using the hypersphere. Additionally, we could also extend the greedy principal boundary to be a maximal margin classifier. Although this has already been done in [4], it has yet to be done with a greedy approach, and would be the first greedy maximal margin classifier for multivariate data lying on some Riemannian manifold.

Bibliography

[1] Borg, I., and Groenen, P. J. F. (2005), textitModern Multidimensional Scaling, Theory and Applications, 2 edn Springer.

[2] Fletcher, P. T., Lu, C., Pizer, S. M., and Joshi, S. (2004), "Principal Geodesic Analysis for the Study of Nonlinear Statistics of Shape," *IEEE Transactions on Medical Imaging*, 23, 995-1005.

[3] Tenenbaum, J. B., Silva, V. D., and Langford, J. C. (2000). "A Global Geometric Framework for Nonlinear Dimensionality Reduction." *Science*, 290: 2319-2323.

[4] Yao, Z., and Zhang, Z. (2019) "Principal Boundary on Riemannian Manifolds."

[5] Panaretos, V. M., Pham, T., and Yao, Z. (2014), "Principal Flows," *Journal of the American Statistical Association*, 109, 424-436.

[6] Roweis, S. T., and Saul, L. K. (2003). "Think Globally, Fit Locally: Supervised Learning of Low Dimensional Manifolds." *Journal of Machine Learning Research*, 4: 119–155.

[7] Conrad Sanderson: Conceptual illustration of the tangent space at point P on a Riemannian manifold.
`https://www.researchgate.net/figure/Conceptual-illustration-of-the-tangent-space-at-point-P-on-a-Riemannian-manifold-M_fig2_262974373`
Accessed: 03/03/2021

[8] Alexwright: Tangent Space Illustration.
https://en.wikipedia.org/wiki/Tangent_space#/media/File:Image_Tangent-plane.svg Accessed: 03/03/2021